Abstract #04551 ISMRM ABSTRACT

Detectability of white matter hyperintensities in 0.6T FLAIR scans

Primary: Physics & Engineering - Low-Field MRI 〉 **Secondary:** Neuro - Aging 〉 **Digital Poster** · 60 min | From Bench to Bedside: All About the Brain in Health and Alzheimer's Disease · Tuesday, May 12 at 09:20 AM 〉 **Keywords:** FLAIR IMAGING WHITE MATTER HYPERINTENSITY MID-FIELD MRI BRAIN LESION VOLUME BRAIN LESION DETECTABILITY

Navid Jabarimani [1,2], **Jeroen de Bresser**[2], **Ece Ercan**[3], **Marius Staring**[2], **Matthias van Osch**[1], **Martijn Nagtegaal**[1]

[1]Department of Radiology, C.J. Gorter MRI Center, Leiden University Medical Center, Netherlands
[2]Department of Radiology, Leiden University Medical Center, Leiden, Netherlands
[3]Philips Healthcare, Best, Netherlands

Presenting Author: *Navid Jabarimani (n.jabarimani@lumc.nl)*

Impact

0.6T MRI potentially enables detecting WMH and estimating WMH burden.

Synopsis

Motivation: Midfield MRI can improve accessibility but suffers from reduced contrast and SNR. It is essential to understand its performance for pathology detection.

Goals: To evaluate the reliability of 0.6T FLAIR MRI for detecting white matter hyperintensities (WMHs) against 1.5T.

Approach: Five older adult volunteers were scanned on both field strengths. Lesions were segmented with LST-AI, manually corrected, and matched voxel-wise across scanners.

Results: WMHs were visible on both fields with 96–98% volumetric agreement; 64% of variation arose from matched lesions. Smaller lesions were more often unmatched.

Introduction

Midfield MR scanners (0.1-1T) have great potential for making MRI more accessible because of reduced exclusion criteria, increased comfort, and healthcare expense benefits[1,2]. Reducing the magnetic field strength has the downside of image contrast changes and reduction in signal-to-noise ratio compared to standard clinical MRI scanners [3,4].

White Matter Hyperintensities (WMH) that can be seen on Fluid Attenuated Inversion Recovery (FLAIR) MRI scans commonly occur in normal brain aging and are an important marker of small vessel disease. Furthermore, WMHs are related to cognitive impairment and are a risk factor for dementia and stroke[5–7]. The goal of this study was to assess and quantify the detectability of WMHs at 0.6T in comparison to standard 1.5T.

Methods

In this study, five healthy older adult volunteers (age=64-75 years) were scanned on a prototype BlueSeal 0.6T Philips scanner equipped with 45mT/m, 200T/m/s gradients and a 1.5T Ingenia Ambition X scanner (Philips). A 3DT_1-TFE (1.2 mm isotropic) and a 2D-FLAIR (1.2x1.2x5.0mm^3) scan were acquired on each scanner. Compressed Sense AI was used for denoising. FLAIR inversion time and TR were adjusted for 0.6T due to lower T_1. (0.6T/1.5T:TI=2s/2.5s,TR=6.5s/8.5s,Acceleration=1/1.3,FOV=230/183/120mm,3min02/2min33).

We employed a semi-automated lesion segmentation approach using the LST-AI toolbox [8,9] with registered FLAIR and T1-weighted images as input. The resulting masks were manually corrected in random order under the supervision of an experienced neuroradiologist, following the STRIVE criteria[10,11].

To compare lesion volumes and match WMHs across field strengths, each lesion was individually labeled. The 1.5T FLAIR scans and masks were rigidly registered to the 0.6T scans. Lesions sharing at least one overlapping voxel were considered matched. To account for minor registration errors, single-slice unmatched lesions were checked for adjacent single-slice lesions and matched correspondingly. Registrations were performed using SPM[12] (T1w to FLAIR) and Elastix[13](1.5T FLAIR and mask to 0.6T). Large lesions that were divided into multiple labels were merged (Fig1).

Results

As expected 0.6T FLAIR images exhibited lower contrast and SNR than 1.5T, yet WMHs were clearly visible at both field strengths (Fig.1-2 ▼). In Fig.1, matched lesion groups overlapped across multiple slices, indicating good spatial correspondence. Visual inspection revealed minor shape differences (Fig.2): lesions appeared sharper with clearer intensity transitions on 1.5T, while at 0.6T they were smoother and less distinct. As marked by red arrows (Fig.2), some 0.6T lesions were less hyperintense and near gray matter, reducing conspicuity. Larger lesions were consistently matched across field strengths (Fig.4).

Quantitatively, both total lesion count and volume were higher at 1.5T (ΔN_{all}= 66; ΔV_{all}= 9.6 cm³;Fig3**(Table 1)**). Matched lesions represented 96.3% and 98.4% of the total lesion volume at 1.5T and 0.6T, respectively, demonstrating strong volumetric correspondence between scanners. Most unmatched lesions were small, accounting for 22% and 42% of the total lesion numbers and 1.5% and 3% of total lesion volumes at 0.6T and 1.5T. Approximately 64% of the total volumetric variation ($\Delta V_{matched}$ / ΔV_{all}) originated from differences within the matched lesions themselves, reflecting minor shape and boundary variations rather than detection errors.

Agreement in lesion volume measurements between field strengths was assessed using a Bland–Altman plot (Fig.5). The mean bias was −0.047 cm³, indicating slightly larger lesion volumes on 1.5T, with 95% limits of agreement from −0.363 cm³ to 0.269 cm³.

Discussion

As expected, we observed differences in image contrast and SNR across field strengths, caused by underlying T1 differences. Similar findings have been reported in previous studies comparing mid- and high-field MRI[3,4]. Despite these differences, our results demonstrate a strong agreement in total WMH

volume between 0.6T and 1.5T, which is the primary measure of WMH burden. Mostly, smaller WMH were missed, which didn't contribute much to the total WMH volume/burden. Roughly two-thirds of the total WMH volume variation could be attributed to differences within matched lesions, which may partly result from minor shape discrepancies and especially the sharper lesion appearance at 1.5T.

Regarding lesion count, the higher number of unmatched lesions on 1.5T images was expected and aligns with previous 1.5T–3T studies, where 1.5T detected roughly one-third of the lesions seen at 3T, partly attributed to slice thickness differences[6]. We observe that all the large lesions were matched across field strengths, but smaller ones were more frequently unmatched. Most likely, the higher count on 1.5T can be attributed to its higher contrast, facilitating the detection of smaller lesions with constant slice thickness.

Conclusion

Our findings demonstrate that 0.6T MRI can be used for detecting and quantifying WMHs, even with relatively low lesion load. In agreement with the literature, while smaller lesions are better detected with higher field strength, this has little effect on overall lesion burden.

Acknowledgements

This collaboration project (specifically MN and YD) is co-funded by the PPS Allowance made available by Health~Holland, Top Sector Life Sciences & Health, to stimulate public-private partnerships. This project is a collaboration between Philips and LUMC.

References

1. Campbell-Washburn AE, Ramasawmy R, Restivo MC, et al. Opportunities in Interventional and Diagnostic Imaging by Using High-Performance Low-Field-Strength MRI. Radiology. 2019;293(2):384-393. doi:10.1148/radiol.2019190452

2. Arnold TC, Freeman CW, Litt B, Stein JM. Low-field MRI: Clinical promise and challenges. Magnetic Resonance Imaging. 2023;57(1):25-44. doi:10.1002/jmri.28408

3. Marques JP, Simonis FFJ, Webb AG. Low-field MRI: An MR physics perspective. J Magn Reson Imaging. 2019;49(6):1528-1542. doi:10.1002/jmri.26637

4. Jabarimani N, Ercan E, Dong Y, et al. Characterizing differences between white and gray matter T W-based segmentations at 0.6 T and 1.5 T.

5. Bachmann R, Reilmann R, Schwindt W, Kugel H, Heindel W, Krämer S. FLAIR imaging for multiple sclerosis: a comparative MR study at 1.5 and 3.0 Tesla. Eur Radiol. 2006;16(4):915-921. doi:10.1007/s00330-005-0070-8

6. Ghaznawi R, Geerlings MI, Jaarsma-Coes M, Hendrikse J, De Bresser J, on behalf of the UCC-Smart Study Group F.L.J. Visseren MD, PhD F.W. Asselbergs MD, PhD H.M. Nathoe MD, PhD M.L. Bots MD, PhD M.H. Emmelot MD, PhD G.J. de Borst MD, PhD L.J. Kappelle MD, PhD T. Leiner MD, PhD P.A. de Jong MD, PhD A.T. Lely MD, PhD N.P. van der Kaaij MD, PhD Y. Ruigrok MD, PhD M.C. Verhaar MD, PhD J. Westerink MD, PhD. Association of White Matter Hyperintensity Markers on MRI and Long-term Risk of Mortality and Ischemic Stroke: The SMART-MR Study. Neurology. 2021;96(17). doi:10.1212/WNL.0000000000011827

7. Keller JA, Sigurdsson S, Klaassen K, et al. White matter hyperintensity shape is associated with long-term dementia risk. Alzheimer's & Dementia. 2023;19(12):5632-5641. doi:10.1002/alz.13345

8. Heinen R, Steenwijk MD, Barkhof F, et al. Performance of five automated white matter hyperintensity segmentation methods in a multicenter dataset. Sci Rep. 2019;9(1):16742. doi:10.1038/s41598-019-52966-0

9. Wiltgen T, McGinnis J, Schlaeger S, et al. LST-AI: A deep learning ensemble for accurate MS lesion segmentation. NeuroImage: Clinical. 2024;42:103611. doi:10.1016/j.nicl.2024.103611

10. Duering M, Biessels GJ, Brodtmann A, et al. Neuroimaging standards for research into small vessel disease—advances since 2013. The Lancet Neurology. 2023;22(7):602-618. doi:10.1016/S1474-4422(23)00131-X

11. Wardlaw JM, Smith EE, Biessels GJ, et al. Neuroimaging standards for research into small vessel disease and its contribution to ageing and neurodegeneration. The Lancet Neurology. 2013;12(8):822-838. doi:10.1016/S1474-4422(13)70124-8

12. Ashburner J, Friston K. CHAPTER 4 - Rigid Body Registration. In: FRISTON K, ASHBURNER J, KIEBEL S, NICHOLS T, PENNY W, eds. Statistical Parametric Mapping. Academic Press; 2007:49-62. doi:10.1016/B978-012372560-8/50004-8

13. Klein S, Staring M, Murphy K, Viergever MA, Pluim J. elastix: A Toolbox for Intensity-Based Medical Image Registration. IEEE Trans Med Imaging. 2010;29(1):196-205. doi:10.1109/TMI.2009.2035616

Figures and Tables

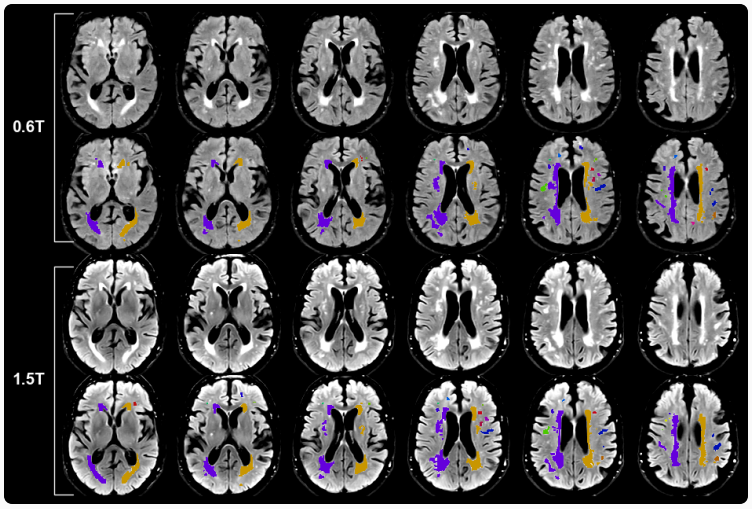

Scan for high-resolution version

Figure 1: *FLAIR scans at 0.6T and 1.5T showing WMHs with corresponding color-coded segmentations. Each isolated segmentation was assigned an ID, and connected lesions were grouped; 20 example groups are represented with different colors.*

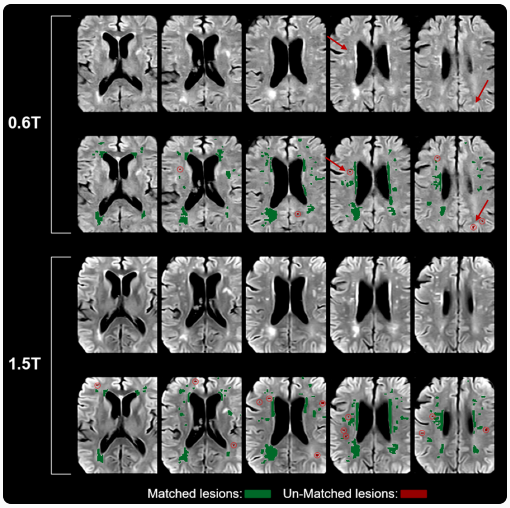

Scan for high-resolution version

Figure 2: *Matched and unmatched lesions in one subject. Small unmatched lesions occurred at both fields; at 0.6T, most were detection errors—some likely due to AI reconstruction artifacts, while others that were near gray matter areas likely arose from reduced tissue contrast.*

Subject	All lesions count [Volume cm³]		Matching lesions count [Volume cm³]		Unmatched lesions count [Volume cm³]	
	1.5T	0.6T	1.5T	0.6T	1.5T	0.6T
vol 1	65 [19.76]	39 [16.75]	31 [18.8]	31 [16.53]	34 [0.96]	8 [0.22]
vol 2	22 [6.28]	17 [4.8]	8 [5.24]	8 [4.47]	14 [1.05]	9 [0.33]
vol 3	72 [20.27]	59 [18.03]	50 [19.52]	50 [17.78]	22 [0.75]	9 [0.25]
vol 4	27 [9.02]	21 [8.9]	13 [8.54]	13 [8.48]	14 [0.49]	8 [0.42]
vol 5	73 [52.59]	57 [49.84]	48 [51.83]	48 [49.57]	25 [0.76]	9 [0.27]
Total	259 [107.92]	193 [98.32]	150[103.93]	150 [96.83]	109 [4.01]	43 [1.49]
Mean ± SD	51.80 ± 22.52 [21.58 ± 16.48]	38.60 ± 17.50 [19.66 ± 15.87]	30.00 ± 17.31 [20.79 ± 16.50]	30.00 ± 17.31 [19.37 ± 15.89]	21.80 ± 7.49 [0.80 ± 0.19]	8.60 ± 0.49 [0.30 ± 0.07]

Scan for high-resolution version

Figure 3: *Counts and volumes of all lesions at both field strengths in 5 different participants. Unmatched 0.6T lesions were detected only on 0.6T, while unmatched 1.5T lesions appeared only on 1.5T without overlap across scanners. this table shows that unmatched lesions accounted for only 1.5% and 3% and matched lesions accounted for 98.4% and 96.3% of total lesions volume at 0.6T and 1.5T.*

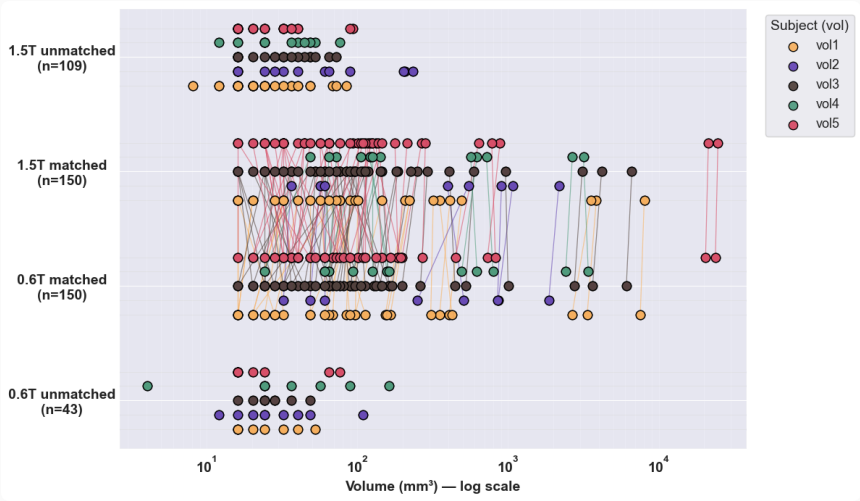

Scan for high-resolution version

Figure 4: *Distribution of matched and unmatched lesions plotted against the log of lesion volume. The figure shows more matched lesions, especially at larger volumes. Connection lines link each lesion to its counterpart across field strengths, which are reflecting minor volume differences between matches.*

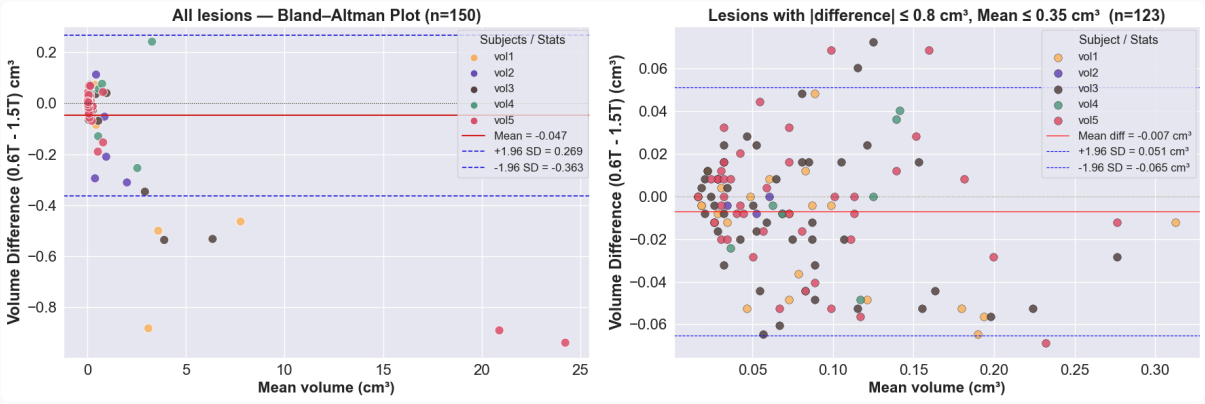

Scan for high-resolution version

Figure 5: *Bland–Altman plots of matched lesions. The left panel includes all lesions, while the right focuses on smaller ones. The plots show minor volume differences, with the mean bias indicating a slight underestimation of 0.6T lesion volumes.*